Two-Step and Reversible Phase Transitions of Organic Polymer Crystals Produced by Topochemical Polymerization

Akikazu Matsumoto*,†,‡ and Hideyuki Nakazawa‡

Department of Applied Chemistry, Graduate School of Engineering, Osaka City University, and PRESTO, Japan Science and Technology Corporation Agency (JST), Sugimoto, Sumiyoshi-ku, Osaka 558-8585, Japan

Received June 3, 2004; Revised Manuscript Received August 18, 2004

ABSTRACT: We describe here the novel phase transition of organic polymer crystals that are directly fabricated by the topochemical polymerization of the 4-bromo- and 4-chlorobenzyl esters of (*Z,Z*)-muconic acid as the 1,3-diene monomers in the crystalline state. The obtained polymers are thermally stable, and their crystal structures reversibly change in two steps according to the temperature. The phase transition of the organic polymer crystals has been revealed on the basis of the results of thermal analyses including thermogravimetric analysis (TG), differential thermal analysis (DTA), and differential scanning calorimetry (DSC), as well as powder X-ray diffraction (XRD), single-crystal structure analysis, and IR spectroscopy under temperature control. We have evaluated a change in cell lengths from *d*-spacing values observed by XRD at various temperatures and concluded that the conformational change in the ester moiety of the polymer side chain induces a noncontinuous change in the crystal structures as the phase transition, which can be detected by X-ray diffraction measurement and thermal analyses.

Introduction

Phase transitions are important for basic science and applied technology because they include a noncontinuous change in the structure and the physical properties of organic materials including crystalline polymers in the solid state.[1−3] Crystalline materials can exist in two or more polymorphic forms, and the process of transformation from one polymorph to another is a phase transition.[4−11] For the crystals of low-molecular-weight organic compounds, polymorphs are often found, according to a procedure and conditions for a crystallization process such as the temperature, solvent, seed, and crystal growth rate.[4−7] Furthermore, the phase transitions of liquid crystals consisting of organic compounds and polymers are used for many applications in a wide range of fields such as display, films, optoelectronics, and photonics.[8,9] In contrast, a few cases were reported as reversible transitions between two different crystal structures for organic materials in the solid state, because of the thermal and mechanical instability of low-molecular-weight organic solids; that is, melting, sublimation, and decomposition occur upon heating, as well as the collapse of the crystalline structure. For crystalline polymers, polymorph is often observed, and the crystallization or ordering process of polymer chains has been intensively investigated as well as their physical properties.[10,11] However, many studies have been carried out using partly crystalline polymer samples, because of the lack of growth into a single crystal in a sufficient size for the determination of a structure and the evaluation of physical properties.

Crystal engineering is the planning and construction of the structures and properties of crystalline materials by designing molecular building blocks in a desired packing structure through intermolecular interactions.[12,13] It is applied to the architecture of polymeric crystalline material consisting of well-controlled chain and crystal structures. Topochemical polymerization proceeds via a specific crystal-to-crystal reaction mechanism, leading to the formation of polymer crystals that cannot be manufactured by the crystallization of a preformed polymer.[14−24] For polymers containing a partly crystalline structure, the detail of the change in crystal structure is sometimes illegible due to the presence of amorphous regions. In contrast, polymer crystals produced by topochemical polymerization have a high quality in their crystallinity. In addition, the polymer chains have a fully extended chain conformation, which is different from a folded structure for flexible polymer chains in lamellar crystals. Therefore, the topochemically prepared polymer crystals are suitable as model crystals to study the structure and properties of common crystalline polymers. Tashiro and co-workers[25−27] have recently revealed the crystalline structure and mechanical properties of regularly and partly crystalline poly(diethyl muconate)s. More recently, we have found a novel feature of polymeric crystals with an excellently ordered chain structure and conformation, which are distinguished from common crystalline polymers. Polymer crystals obtained by the topochemical polymerization of the 4-bromo- and 4-chlorobenzyl esters of (*Z,Z*)-muconic acid, poly(**1**) and poly(**2**) in Chart 1, are thermally stable, and their crystal structures clearly and reversibly change in two steps according to the temperature conditions. In this paper, the novel phase transition of the organic polymer crystals is revealed on the basis of thermal analyses including thermogravimetric analysis (TG), differential thermal analysis (DTA), and differential scanning calorimetry (DSC), as well as powder X-ray diffraction (XRD), single-crystal structure analysis, and IR spectroscopy under temperature control.

Experimental Section

General Methods. NMR and UV spectra were recorded on JEOL JNM A-400 and JASCO V-550

* Corresponding author. Fax: +81-6-6605-2981. E-mail: matsumoto@a-chem.eng.osaka-cu.ac.jp.
† PRESTO-JST.
‡ Osaka City University.

10.1021/ma048905a CCC: $27.50
Published on Web 10/21/2004

Chart 1

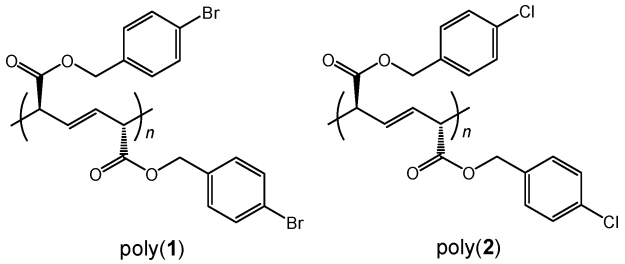

poly(**1**) poly(**2**)

spectrometers, respectively, at an ambient temperature. IR spectrum was recorded on a JASCO Herschel FT-IR-670 Plus spectrometer equipped with Irtron IRT-30 and a temperature control unit. The sample was sandwiched between KBr plates, pressed, and then measured for transmittance over the temperature rage 50−250 °C at a heating and cooling rate of 10 °C/min. The powder X-ray diffraction profile was recorded on a Rigaku RINT-2100 with monochromatized Cu Kα radiation (λ = 1.54184 Å, 40 kV, 40 mA, scan speed 2.0°/min, scan range 3−40°) under temperature control, equipped with a high-resolution parallel-beam optics system consisting of a parallel slip analyzer PSA100U and a graded multiplayer 2960C1. Single-crystal X-ray data were collected on a Rigaku R-AXIS RAPID Imaging Plate diffractometer using Mo Kα radiation monochromatized by graphite (λ = 0.71073 Å). The structures were solved by a direct method with the program SIR92 and refined using full-matrix least-squares procedures. All calculations were performed using the CrystalStructure crystallographic software package. The simultaneous measurement of XRD and DSC was carried out with a Rigaku RINT-Ultima II equipped with a DSC attachment (Cu Kα, 40 kV, 50 mA, scan speed 0.7°/min, scan range 4−6°, heating and cooling rate 1 °C/min, the flow rate of dry nitrogen gas 30 mL/min). TG/DTA analysis was carried out with Seiko TG-6200 in a nitrogen stream at a heating rate of 10 °C/min over a range from room temperature to 500 °C. The initial decomposition temperature (T_{init}) was evaluated as the temperature at which 5 wt % weight loss was observed. The maximum decomposition temperature (T_{max}) was determined from a differential thermogravimetric curve in TG analysis. DSC analysis was carried out with Seiko DSC-6200 in a nitrogen atmosphere at a heating and cooling rate of 1, 10, or 20 °C/min. Transition temperatures (T_1 and T_2) and a melting temperature (T_m) were determined as the peak temperatures of the DTA or DSC curve.

Materials. Bis(4-bromobenzyl) (*Z,Z*)-muconate (**1**) was prepared by the method described in previous papers.[28,29] To (*Z,Z*)-muconic acid (1.42 g, 10.0 mmol) in 10 mL of hexamethylphosphoramide (HMPA) in a 100 mL flask equipped with a calcium chloride tube were added 4-bromobenzyl bromide (5.03 g, 20.1 mmol) and potassium carbonate (3.50 g, 25.3 mmol), and the mixture was stirred at room temperature for 1 day. The reaction mixture was poured into 500 mL of saturated brine, and the crude product was extracted with two portions of 100 mL of chloroform. After the chloroform solution was washed with water and then dried over sodium sulfate, the chloroform was evaporated under reduced pressure, providing a colorless solid. The precipitated solid was filtered and dried under reduced pressure; silica gel column chromatography with chloroform as the eluent provided bis(4-bromobenzyl) (*Z,Z*)-muconate. Yield 4.04 g (84.1%). Bis(4-chlorobenzyl) (*Z,Z*)-muconate (**2**) was also similarly prepared. Yield: 3.87 g (80.5%). Melting point and spectral data are as follows.

1: mp 142.0−142.4 °C ($CHCl_3$); ^{1}H NMR (400 MHz, $CDCl_3$) δ 7.92 (m, C*H*=CHCO$_2$R, 2H), 7.49 (m, C_6H_4, 4H), 7.25 (m, C_6H_4, 4H), 6.02 (m, CH=C*H*CO$_2$R, 2H), 5.13 (s, OCH_2, 4H); ^{13}C NMR (100 MHz, $CDCl_3$) δ 165.15 (C=O), 138.49 (CH=), 134.67, 131.74, 129.92, 122.40 (C_6H_4), 123.86 (CH=), 65.59 (CH_2); UV(acetonitrile) λ_{max} 260 nm (ϵ = 26 100); IR (KBr) 1710 ($\nu_{C=C}$), 1584 ($\nu_{C=O}$) cm^{-1}.

2: mp 130.8−131.0 °C ($CHCl_3$); ^{1}H NMR (400 MHz, $CDCl_3$) δ 7.92 (m, C*H*=CHCO$_2$R, 2H), 7.32 (m, C_6H_4, 8H), 6.02 (m, CH=C*H*CO$_2$R, 2H), 5.14 (s, OCH_2, 4H); ^{13}C NMR (100 MHz, $CDCl_3$) δ 165.15 (C=O), 138.46 (CH=), 134.21, 134.15, 129.62, 128.77 (C_6H_4), 123.86 (CH=), 65.42 (CH_2); UV (acetonitrile) λ_{max} 261 nm (ϵ = 24 300); IR (KBr) 1712 ($\nu_{C=C}$), 1588 ($\nu_{C=O}$) cm^{-1}.

The monomer crystals were photoirradiated with a high-pressure mercury lamp (Toshiba SHL-100-2, 100 W, Pyrex filter) at a distance of 10 cm under atmospheric conditions at room temperature. After irradiation, the resulting polymers were isolated by removal of the unreacted monomer with chloroform. The polymer yield was gravimetrically determined. For fabrication of polymer single crystals, monomer single crystals were cut to an appropriate size and charged into a Pyrex tube, degassed, and then sealed. γ-Radiation was carried out with ^{60}Co at room temperature at the Research Institute for Advanced Science and Technology (RIAST), Osaka Prefecture University. The irradiation dose was 200 kGy. After irradiation, the quantitative polymer formation was examined by IR spectroscopy and used for the X-ray structure analysis.

Crystallographic Data. The summary of the single-crystal structure analysis of poly(**1**) at various temperatures is as follows.

Temp −70 °C, monoclinic, space group $P2_1/c$, a = 5.811(2) Å, b = 4.857(1) Å, c = 32.313(9) Å, β = 90.49(2)°, V = 912.1(4) Å^3, Z = 2, ρ_{calc} = 1.748 g/cm^3, unique reflections 2086, number observed ($I > 2.0\sigma(I)$) 1614, R = 0.077, R_w = 0.125, GOF = 1.17, $2\theta_{max}$ = 55.0°, R/P = 12.81.

Temp −50 °C, monoclinic, space group $P2_1/c$, a = 5.823(2) Å, b = 4.864(1) Å, c = 32.375(7) Å, β = 90.68(2) °, V = 916.8(4) Å^3, Z = 2, ρ_{calc} = 1.739 g/cm^3, unique reflections 2099, number observed ($I > 2.0\sigma(I)$) 1594, R = 0.073, R_w = 0.113, GOF = 1.28, $2\theta_{max}$ = 55.0°, R/P = 12.65.

Temp −30 °C, monoclinic, space group $P2_1/c$, a = 5.816(2) Å, b = 4.855(1) Å, c = 32.467(8) Å, β = 90.67(1)°, V = 916.7(4) Å^3, Z = 2, ρ_{calc} = 1.739 g/cm^3, unique reflections 2083, number observed ($I > 2.0\sigma(I)$) 1575, R = 0.069, R_w = 0.112, GOF = 1.31, $2\theta_{max}$ = 55.0°, R/P = 12.50.

Temp −10 °C, monoclinic, space group $P2_1/c$, a = 5.813(1) Å, b = 4.856(1) Å, c = 32.475(7) Å, β = 90.77(1)°, V = 916.6(4) Å^3, Z = 2, ρ_{calc} = 1.740 g/cm^3, unique reflections 2084, number observed ($I > 2.0\sigma(I)$) 1546, R = 0.066, R_w = 0.112, GOF = 1.21, $2\theta_{max}$ = 54.9°, R/P = 12.27.

Temp 10 °C, monoclinic, space group $P2_1/c$, a = 5.828(2) Å, b = 4.855(1) Å, c = 32.644(8) Å, β = 90.92(1)°, V = 923.5(4) Å^3, Z = 2, ρ_{calc} = 1.727 g/cm^3, unique reflections 2093, number observed ($I > 2.0\sigma(I)$)

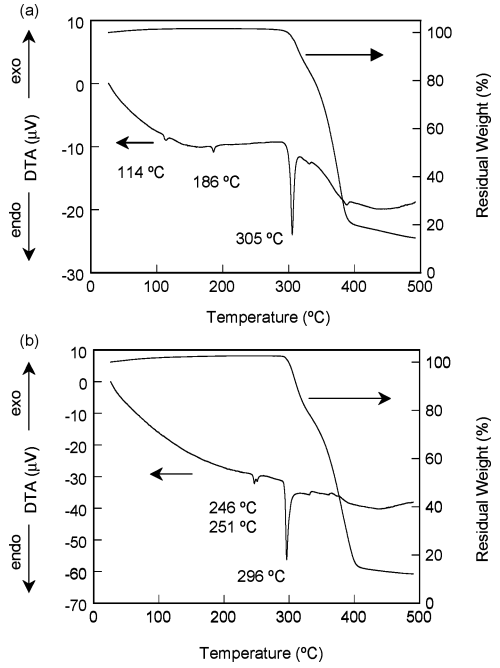

Figure 1. TG/DTA curves of the crystal of (a) poly(**1**) and (b) poly(**2**). A heating rate of 10 °C/min in nitrogen stream.

1478, $R = 0.067$, $R_w = 0.098$, GOF = 1.19, $2\theta_{max} = 55.0°$, $R/P = 11.73$.

Temp 30 °C, monoclinic, space group $P2_1/c$, a = 5.837(2) Å, b = 4.856(1) Å, c = 32.742(9) Å, β = 91.05(2)°, V = 927.8(5) Å^3, $Z = 2$, ρ_{calc} = 1.719 g/cm^3, unique reflections 2095, number observed ($I > 2.0\sigma(I)$) 1456, $R = 0.064$, $R_w = 0.091$, GOF = 1.20, $2\theta_{max} = 55.0°$, $R/P = 11.56$.

Temp 50 °C, monoclinic, space group $P2_1/c$, a = 5.842(2) Å, b = 4.854(1) Å, c = 32.845(9) Å, β = 91.17(2)°, V = 931.2(5) Å^3, $Z = 2$, ρ_{calc} = 1.712 g/cm^3, unique reflections 2109, number observed ($I > 2.0\sigma(I)$) 1391, $R = 0.063$, $R_w = 0.088$, GOF = 1.16, $2\theta_{max} = 54.9°$, $R/P = 11.04$.

Temp 70 °C, monoclinic, space group $P2_1/c$, a = 5.796(2) Å, b = 4.880(1) Å, c = 32.6686(8) Å, β = 91.11(2)°, V = 924.4(4) Å^3, $Z = 2$, ρ_{calc} = 1.725 g/cm^3, unique reflections 2112, number observed ($I > 2.0\sigma(I)$) 1399, $R = 0.068$, $R_w = 0.102$, GOF = 1.17, $2\theta_{max} = 55.0°$, $R/P = 11.10$.

Temp 90 °C, monoclinic, space group $P2_1/c$, a = 5.821(2) Å, b = 4.869(1) Å, c = 32.886(8) Å, β = 91.19(1)°, V = 931.9(4) Å^3, $Z = 2$, ρ_{calc} = 1.711 g/cm^3, unique reflections 2091, number observed ($I > 2.0\sigma(I)$) 1307, $R = 0.064$, $R_w = 0.086$, GOF = 1.12, $2\theta_{max} = 54.7°$, $R/P = 10.37$.

Temp 110 °C, monoclinic, space group $P2_1/c$, a = 5.824(2) Å, b = 4.857(2) Å, c = 32.96(1) Å, β = 91.04(1)°, V = 932.0(5) Å^3, $Z = 2$, ρ_{calc} = 1.711 g/cm^3, unique reflections 2064, number observed ($I > 2.0\sigma(I)$) 1232, $R = 0.063$, $R_w = 0.090$, GOF = 1.16, $2\theta_{max} = 54.5°$, $R/P = 9.78$.

Results and Discussion

Thermal Analyses. Thermogravimetric (TG) and differential thermal analyses (DTA) were carried out for poly(**1**) and poly(**2**) at a heating rate of 10 °C/min in a nitrogen stream. The results are shown in Figure 1 and Table 1. Both polymer crystals were thermally stable and neither decomposed nor melted under approximately 300 °C. They showed a clear melting point due to their extremely high crystallinity: T_m = 305 and 296 °C for poly(**1**) and poly(**2**), respectively. In their DTA traces, small endothermic peaks were observed at 114.4 and 186.0 °C for poly(**1**), and 246.7 and 250.9 °C for poly(**2**) due to any transitions below the melting points or the onset temperature of decomposition. Therefore, we further investigated the transitions by DSC analysis. The results of DSC data obtained under various scanning conditions are summarized in Table 2. The transition temperatures observed in the first run (T_1 = 115.1 °C and T_2 = 186.6 °C) were consistent with the DTA results (Table 1), when the polymers were used in the form as polymerized after removing the unreacted monomer with chloroform at room temperature. This T_1 value in the first run was higher than that observed for those in the second and third runs (T_1 = 105.9 and 105.7 °C, respectively). These thermodynamic changes in the DSC traces were reversible, but the transition was always observed at a lower temperature in the cooling process than that in the heating process; endothermic and exothermic peaks were observed at 105.9 and 186.6 °C (ΔH = 6.1 and 5.4 mJ/unit, respectively) upon heating, and 86.5 and 182.6 °C (ΔH = −5.3 and −5.4 mJ/unit, respectively) upon cooling, as shown in the thermogram for poly(**1**) (Figure 2). The results of DSC experiments with different heating rates (1, 10, and 20 °C/min) indicate that this transition process is independent of the measurement conditions such as the scanning rate (Figure 2b and Table 2).

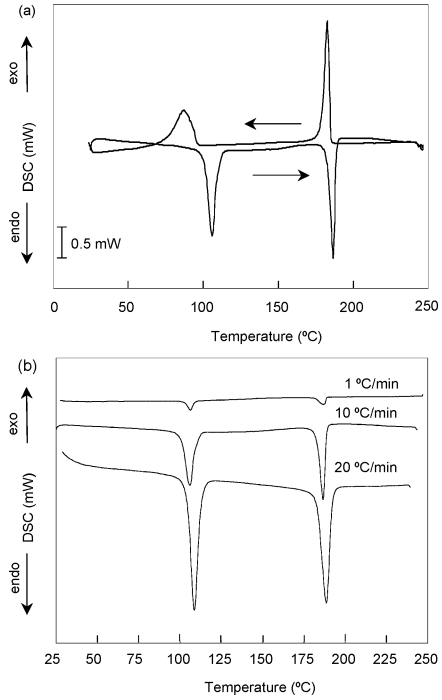

Figure 2. DSC traces of the crystal of poly(**1**) (second run). (a) Heating and cooling rate of 10 °C/min in nitrogen stream. (b) Effect of the heating rate.

Table 1. TG/DTA Data for Poly(1) and Poly(2)

	TG		DTA		
polymer	T_{init} (°C)	T_{max} (°C)	T_1 (°C)	T_2 (°C)	T_m (°C)
poly(**1**)	298.5	313.0	114.4	186.0	305.4
poly(**2**)	299.2	309.1	246.7	250.9	296.3

XRD and Single-Crystal Structure Analysis. To reveal the structural change due to the phase transitions, powder X-ray diffraction (XRD) patterns were

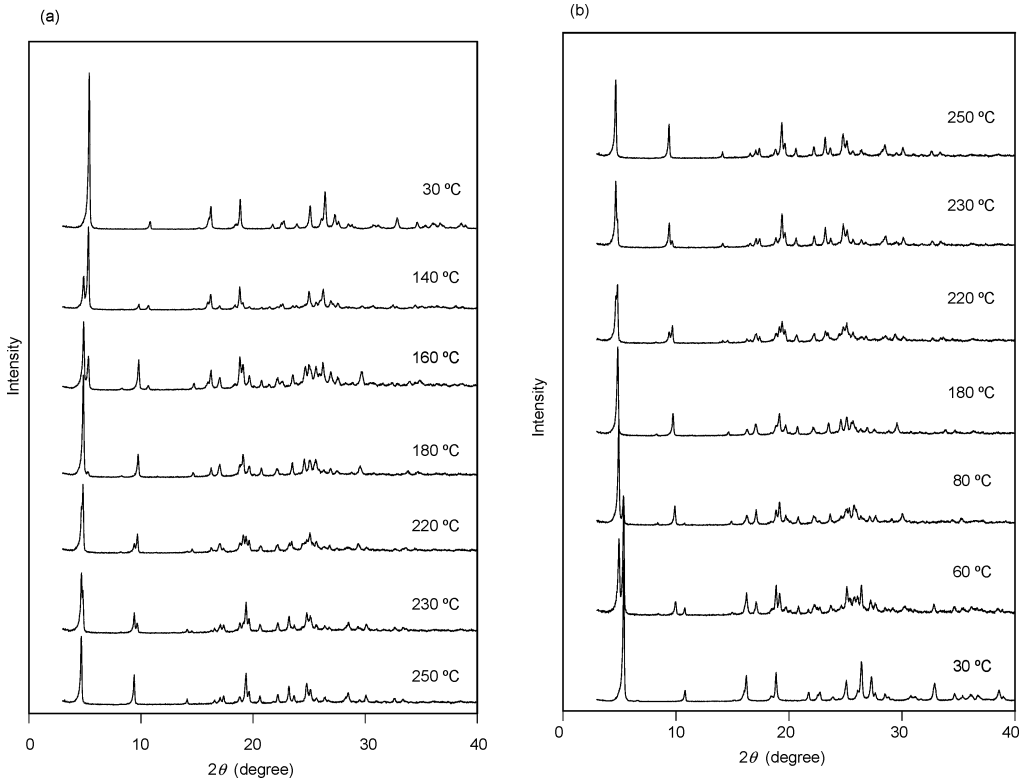

Figure 3. Change in powder X-ray diffraction profiles of poly(**1**) on (a) heating and (b) cooling. The temperature was changed stepwise in the range 30−250 °C. X-ray radiation conditions: Cu Kα, 40 kV, 40 mA, scan speed 2.0°/min, scan range 3−40°.

Table 2. DSC Data for Poly(1)

	on heating					on cooling				
run	rate (°C/min)	T_1 (°C)	ΔH_1 (mJ/unit)	T_2 (°C)	ΔH_2 (mJ/unit)	rate (°C/min)	T_1 (°C)	ΔH_1 (mJ/unit)	T_2 (°C)	ΔH_2 (mJ/unit)
first	10	115.1	4.54	186.6	4.53	10	88.0	−5.54	182.5	−5.71
second	1	106.4	6.08	186.6	5.37					
	10	105.9	6.05	186.6	5.38	10	86.5	−5.28	182.6	−5.42
	20	108.6	6.10	188.6	5.42					
third	10	105.7	6.03	186.6	5.41	10	86.5	−5.11	182.7	−5.51

recorded at various temperatures. Figure 3 shows the diffraction profiles of poly(**1**) recorded over the temperature range of 30−250 °C. When the polymer crystals were heated stepwise from 30 to 250 °C, the diffraction profiles changed in two steps. For example, the intensity of the peak observed at $2\theta = 5.42°$, which corresponds to $d = 16.30$ Å, decreased, and simultaneously another peak appeared at the smaller angle side upon heating. No original peak was observed at 180 °C, and a further increase in the temperature induced another structural change in the crystals, as is clearly shown in the expanded diffractions of XRD in Figure 4. This process was reversible as shown by changes in the diffraction patterns on cooling (Figure 3b and Figure 4b). Similar reversible phase transitions were also observed for poly(**2**) (Figure 5).

The simultaneous measurement of both XRD and DSC was carried out with the same sample to confirm a direct relationship between the thermodynamics and the structural change during the phase transitions of the crystals. The XRD diffraction was recorded in the range of $2\theta = 4-6°$ at a heating and cooling rate of 1 °C/min. During the heating process, endothermic peaks were observed at 113.8 and 188.9 °C, at which temperatures a drastic change in the XRD profile was detected (Figure 6). On cooling from 250 °C to room temperature, a similar structural change was observed accompanying the exothermic peaks at 185.5 and 92.4 °C in a DSC trace. This strongly supports that the thermodynamic behavior is related to the structural change in the crystal lattice of the polymer. It was confirmed that a change in the XRD profile was always observed over a certain temperature range at the peak temperature in DSC analysis, just the same as those observed in Figures 3 and 4. Phase transitions are generally affected by not only thermodynamic but also kinetic factors. Therefore, the time dependence of the XRD patterns was examined in the range of temperatures where the two phases simultaneously coexist. Consequently, however, we observed the constant ratio, independent of the time, of the peak intensities of two components in XRD diffractions observed around the DSC peak temperature. This means that the composition of both structural components is a function of the temperature and that the two phases are in equilibrium with a fast structural change. This conclusion agrees well with the results for the DSC experiments in Figure 2b, indicating that a kinetic factor is not important during the phase transition of these polymer crystals.

We fully assigned XRD data shown in Figures 3 and 5 on the basis of the single-crystal structures of poly(**1**) and poly(**2**). The results of the analysis of XRD diffractions are summarized in Table 3. Figure 7 shows the single-crystal structure of poly(**1**) determined at 30 °C.

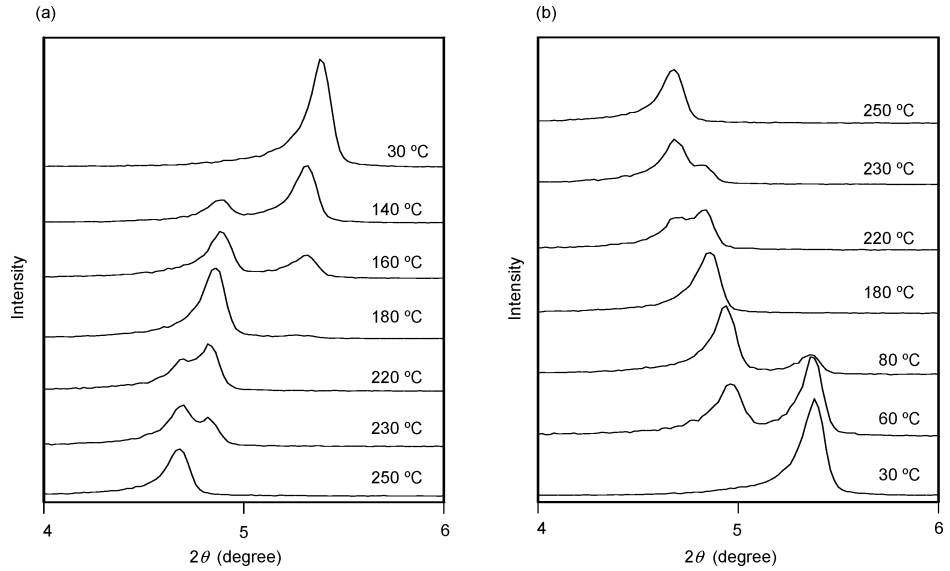

Figure 4. Expanded powder X-ray diffraction profiles of poly(**1**) on (a) heating and (b) cooling. The temperature was changed stepwise in the range 30−250 °C.

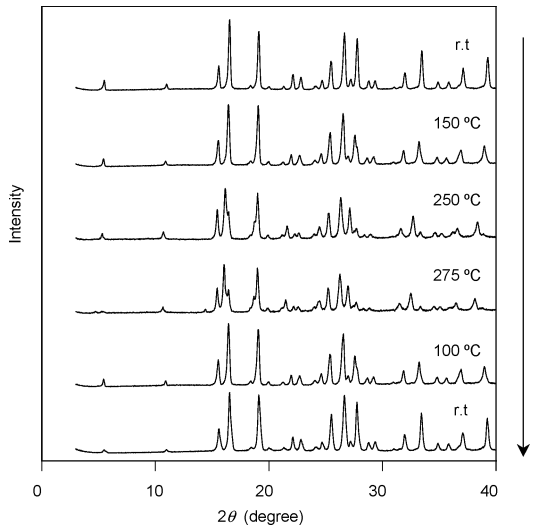

Figure 5. Temperature dependence of X-ray-diffraction profile for poly(**2**) on heating and cooling. The temperature was changed stepwise in the range 30−250 °C.

Molecular packing and chain conformations in the poly(**1**) crystals were very similar to those for poly(**2**) previously reported.[23] Crystallographic data for both polymers are shown in Table 4. Figure 8 shows the XRD profile calculated from the results of the single-crystal structure analysis of poly(**1**) at 30 °C, as well as the observed diffraction profiles before and after a heating and cooling process, as was already shown in Figure 3. These diffraction profiles agree well with each other. The XRD diffractions in Figure 5 were also assigned as is shown in Table 3 in a similar way, on the basis of the single-crystal structure of poly(**2**).

DSC, XRD, and single-crystal structure analysis confirmed no occurrence of phase transition below room temperature to −70 °C, differing from the observation in a higher temperature region. For example, the obtained crystal parameters are as follows: for the structure determined at −70 °C, monoclinic, space group $P2_1/c$, $a = 5.811(2)$ Å, $b = 4.857(1)$ Å, $c = 32.313(9)$ Å, $\beta = 90.49(2)°$, $V = 912.1(4)$ Å^3, $\rho_{calc} = 1.748$ g/cm^3, $Z = 2$, reflections measured 6805, unique reflections 2086, number observed ($I > 2\sigma(I)$) 1614, parameter ratio 12.81, $R = 0.077$, $R_w = 0.125$, GOF = 1.17. For the structure determined at 30 °C, monoclinic, space group $P2_1/c$, $a = 5.837(2)$ Å, $b = 4.856(1)$ Å, $c = 32.742(9)$ Å, $\beta = 91.05(2)°$, $V = 927.8(5)$ Å^3, $\rho_{calc} = 1.719$ g/cm^3, $Z = 2$, reflections measured 6690, unique reflections 2095, number observed ($I > 2\sigma(I)$) 1456, parameter ratio 11.56, $R = 0.064$, $R_w = 0.091$, GOF = 1.20. All the cell parameters continuously change over the range from −70 to +110 °C (see Experimental Section). We also attempted to determine the single-crystal structure of poly(**1**) at a higher temperature, but it failed due to the collapse of single-crystal structure. We are continuing an effort to determine the single structures for the high-temperature phases by the careful measurement and analysis of diffractions below and over the phase transition temperature.

Structural Change in Phase Transition. Using eq 1, we evaluated cell lengths on the basis of the d-spacing in the XRD.

$$\frac{1}{d_{hkl}^2} = \frac{1}{\sin^2\beta}\left(\frac{h^2}{a^2} + \frac{k^2\sin^2\beta}{b^2} + \frac{l^2}{c^2} - \frac{2hl\cos\beta}{ac}\right) \quad (1)$$

First, a c-axis length was determined from the d_{002} values at various temperatures. As has already been shown in Figure 4, the diffraction noncontinuously changes depending on the temperature, and in the boundary regions, two phases are simultaneously observed in the temperature ranges of 130−170 and 200−230 °C. A change in the c-axis length is shown in Figure 9a. Similarly, a- and b-axis lengths were estimated using the d_{102} and the $d_{11\bar{1}}$ values. For the determination of the latter, experimentally obtained values of the angle β were used for the calculation below 110 °C, and the value at 110 °C was used for the estimation of β angles at a higher temperature. The change in the a- and b-axis lengths is shown in Figure 9b,c, respectively. The temperature dependence of the b-axis length and its change accompanied by the transitions were smaller than for the other two axes. This is because of the presence of the covalent chains and intermolecular halogen−halogen interactions along the b-axis. As clearly shown in Figure 7, in the crystals of poly(**1**), the columns of polymer chains are tightly linked by weak

Table 3. XRD Data for Poly(1) and Poly(2)[a]

polymer	temp (°C)	*hkl*	2θ (deg) (calcd)	*d* (Å) (calcd)	height	intensity (%) (calcd)	half-line width
poly(**1**)	30	002	5.417 (5.399)	16.300 (16.368)	9447	100 (100)	0.146
		004	10.84 (10.81)	8.155 (8.184)	555	5.2 (3.7)	0.147
		102	16.24 (16.22)	5.453 (5.465)	1162	16.5 (51.9)	0.238
		011	18.42 (18.47)	4.813 (4.803)	175	2.1 (9.6)	0.235
		104	18.86 (18.84)	4.703 (4.711)	1957	18.4 (57.5)	0.120
		008	21.77 (21.72)	4.079 (4.176)	321	2.9 (0.5)	0.155
		106	22.53 (22.51)	3.944 (3.930)	303	2.4 (8.1)	0.121
		01$\bar{5}$	22.77 (22.80)	3.902 (3.900)	485	5.1 (18.3)	0.167
		11$\bar{1}$	23.93 (23.96)	3.715 (3.714)	220	2.4 (13.5)	0.207
		11$\bar{3}$	25.10 (25.12)	3.545 (3.545)	1220	13.8 (71.3)	0.160
		11$\bar{4}$	26.09 (26.12)	3.412 (3.411)	457	8.7 (25.1)	0.207
		017	26.44 (26.46)	3.369 (3.369)	2099	19.9 (55.4)	0.158
		11$\bar{5}$	27.31 (27.36)	3.262 (3.259)	1005	13.5 (12.7)	0.174
		115	27.61 (27.65)	3.228 (3.227)	340	2.6 (17.0)	0.141
		018	28.51 (28.52)	3.128 (3.129)	296	3.1 (9.2)	0.184
		11$\bar{6}$	28.84 (28.82)	3.093 (3.098)	196	1.6 (9.9)	0.165
		117	30.81 (30.82)	2.900 (2.901)	198	6.3 (5.8)	0.244
		202	31.20 (31.23)	2.864 (2.867)	221	12.4 (4.5)	0.391
		204	32.90 (32.77)	2.720 (2.733)	699	9.4 (10.4)	0.210
		119	34.65 (34.63)	2.587 (2.590)	424	7.3 (10.9)	0.163
		0,1,1$\underline{1}$	35.41 (35.37)	2.533 (2.537)	163	2.4 (2.4)	0.290
		1,0,1$\underline{\bar{2}}$	36.16 (36.09)	2.481 (2.489)	250	5.4 (4.0)	0.432
		1,0,12	36.66 (36.63)	2.449 (2.454)	255	5.5 (4.6)	0.312
		024	38.64 (38.68)	2.328 (2.328)	347	5.9 (1.7)	0.243
		1,1,11	38.95 (38.92)	2.310 (2.314)	188	1.7 (5.8)	0.176
poly(**1**)	180	002	4.874	18.116	1796	100.0	0.142
		004	9.756	9.059	396	20.5	0.146
		102	14.66	6.039	72	3.2	0.153
			16.26	5.447	144	10.0	0.155
			17.02	5.204	196	12.2	0.224
			18.78	4.722	141	10.9	0.212
			19.13	4.635	372	24.9	0.161
		008	19.67	4.509	175	11.4	0.186
			20.75	4.277	138	5.8	0.139
			22.10	4.019	112	8.3	0.255
		11$\bar{1}$	23.51	3.781	225	9.4	0.135
			24.55	3.623	280	16.3	0.149
			25.06	3.550	220	12.7	0.215
			26.95	3.306	82	3.2	0.145
		204	29.54	3.021	134	10.0	0.277
			33.84	2.647	68	7.4	0.226
			34.67	2.586	42	4.3	0.390
poly(**1**)	250	002	4.697	18.80	1283	100.0	0.141
		004	9.395	9.405	577	41.4	0.126
		102	14.12	6.267	95	6.1	0.112
			16.57	5.346	63	5.1	0.133
			17.06	5.193	117	11.1	0.154
			17.37	5.100	155	10.5	0.137
		008	18.89	4.712	125	13.6	0.189
			19.36	4.580	573	40.7	0.146
			19.64	4.516	253	26.2	0.139
			20.62	4.304	146	11.0	0.127
			22.20	4.001	206	20.7	0.112
		11$\bar{1}$	23.20	3.831	351	25.3	0.134
			23.66	3.757	141	9.5	0.140
			24.74	3.596	391	59.9	0.178
			25.11	3.543	265	30.9	0.096
			26.34	3.380	93	12.0	0.170
			28.19	3.163	82	28.9	0.384
		204	28.48	3.132	151	10.4	0.165
			30.07	2.969	154	11.7	0.136
			32.60	2.745	87	6.1	0.169
			33.33	2.686	65	11.1	0.213
poly(**2**)	30	002	5.527 (5.51)	15.978 (16.048)	430	13.2 (6.4)	0.233
		004	11.01 (11.03)	8.031 (8.024)	219	5.9 (1.0)	0.205
		10$\underline{0}$	15.59 (15.60)	5.569 (5.680)	1053	31.3 (55.4)	0.226
		10$\underline{\bar{2}}$	16.54 (16.54)	5.355 (5.360)	3379	100.0 (44.0)	0.225
		10$\bar{4}$	19.11 (19.11)	4.640 (4.643)	2924	89.6 (63.3)	0.233
		013	20.01 (20.06)	4.433 (4.427)	102	2.7 (9.2)	0.201
		014	21.30 (21.36)	4.169 (4.159)	127	2.7 (7.5)	0.159
		00$\underline{8}$	22.12 (22.16)	4.016 (4.012)	711	18.8 (2.1)	0.201
		10$\bar{6}$	22.81 (22.80)	3.894 (3.901)	563	16.8 (5.4)	0.227
		110	24.07 (24.09)	3.694 (3.694)	125	5.1 (10.7)	0.311
		016	24.68 (24.74)	3.605 (3.598)	429	12.1 (10.1)	0.215
		113	25.47 (25.53)	3.494 (3.490)	1378	43.5 (100)	0.240

Table 3 (Continued)

polymer	temp (°C)	*hkl*	2θ (deg) (calcd)	*d* (Å) (calcd)	height	intensity (%) (calcd)	half-line width
poly(**2**)		017	26.66 (26.72)	3.341 (3.336)	2671	92.8 (69.5)	0.264
		108	27.19 (27.25)	3.277 (3.272)	482	19.3 (5.1)	0.305
		11$\bar{5}$	27.76 (27.84)	3.211 (3.205)	2485	74.1 (25.0)	0.227
		018	28.78 (28.85)	3.099 (3.095)	429	13.7 (9.7)	0.243
		116	29.34 (29.41)	3.042 (3.037)	410	12.6 (15.5)	0.233
		11$\bar{7}$	30.04 (31.06)	2.879 (2.880)	75	2.5 (2.8)	0.251
		1,0,$\overline{10}$	31.96 (31.98)	2.798 (2.791)	805	22.3 (0.4)	0.211
		20$\bar{4}$	33.46 (33.43)	2.676 (2.680)	2056	61.5 (10.9)	0.227
		11$\bar{9}$	34.88 (34.93)	2.570 (2.568)	354	11.8 (9.0)	0.253
		0,1,11	35.82 (35.89)	2.505 (2.502)	349	12.0 (4.2)	0.262
		1,0,$\overline{12}$	37.09 (37.11)	2.422 (2.423)	970	28.0 (4.2)	0.220
		1,1,$\overline{11}$	39.26 (39.31)	2.293 (2.292)	1770	61.9 (5.4)	0.266

[a] The values in parentheses are those calculated on the basis of the single-crystal structures of poly(**1**) and poly(**2**).

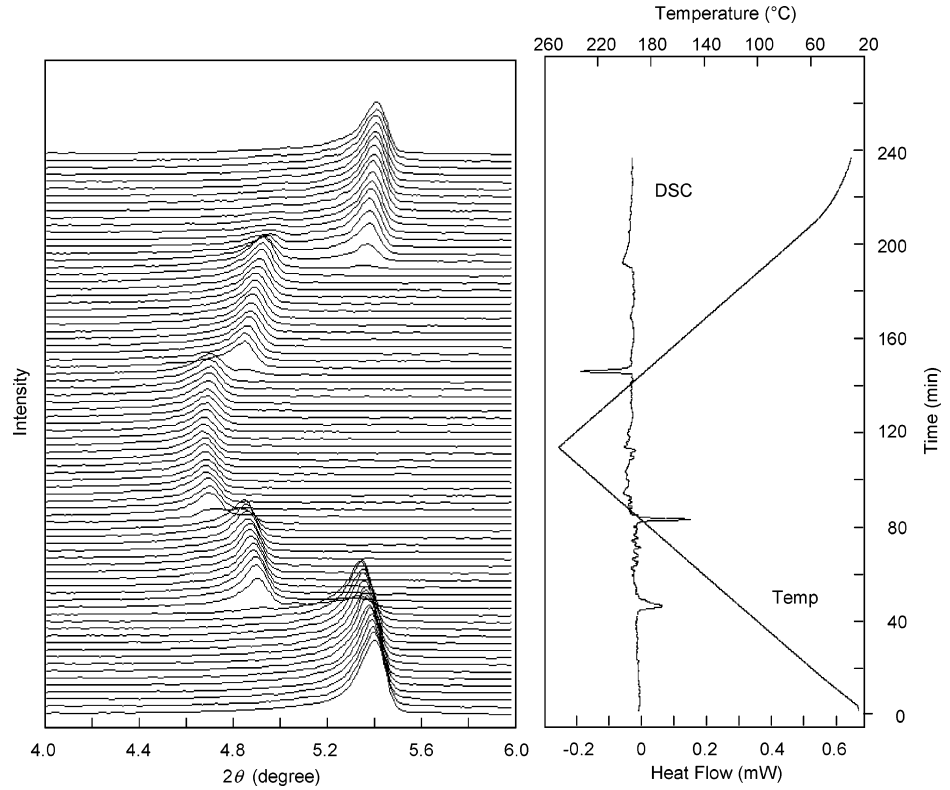

Figure 6. XRD and DSC simultaneous measurements of poly(**1**). Heating and cooling rate of 1 °C /min in a nitrogen stream. X-ray radiation conditions: Cu Kα, 40 kV, 50 mA, scan speed 0.7°/min, scan range 4−6°.

hydrogen bonds between halogen atoms to form two-dimensional polymer sheets. The distance for close contact between the nonbonding chlorine atoms was 3.64 Å, being very similar to that for the monomer crystals (3.63 Å),[23] and shorter than the sum of the corresponding van der Waals radii.[30,31] The polymer sheets are further linked to each other through weak hydrogen bond interaction between the carbonyl carbon and the olefinic hydrogen in the polymer main chain.

The axis lengths for the three phases are summarized in Table 5. Upon heating, the *c*- and *a*-axis lengths increased by 11 and 4% in the phase transitions from the original to the second, and from the second to the third phases, respectively. In contrast, the *b*-axis probably implies less change in the length because of the presence of the rigid polymer chains and halogen zigzag chains. During the cooling process, similar transitions were observed and the identical cell parameters were obtained. A similar reversible phase transition was also observed in poly(**2**), but not in other polymers with other substituents such as an alkoxy group. This suggests the contribution of interchain halogen−halogen interactions for the reversible structural change in the polymer crystals.

We also investigated the temperature dependence of the vibrational modes of the chemical bonds by IR spectroscopy. The absorption bands around 1000 and 1180 cm^{-1} showed extraordinary temperature dependence (Figure 10). On cooling, a reverse change was also observed as was expected. Recently, Nakamoto et al.[25] successfully revealed the mechanical deformation behavior of a giant single crystal of poly(diethyl muconate). IR and Raman spectra were measured as a function of tensile stress for the polymer crystal, which was tensioned along the chain axis. The structural data were analyzed on the basis of normal-modes calculation under a quasi-harmonic approximation, allowing the estimating of the microscopic deformation mechanism of the polymer chain under tension. Similarly, the absorption bands shown in Figure 10 in the present work are assigned to the vibrational stretching due to several C−C and C−O bonds. The peaks observed around 1000

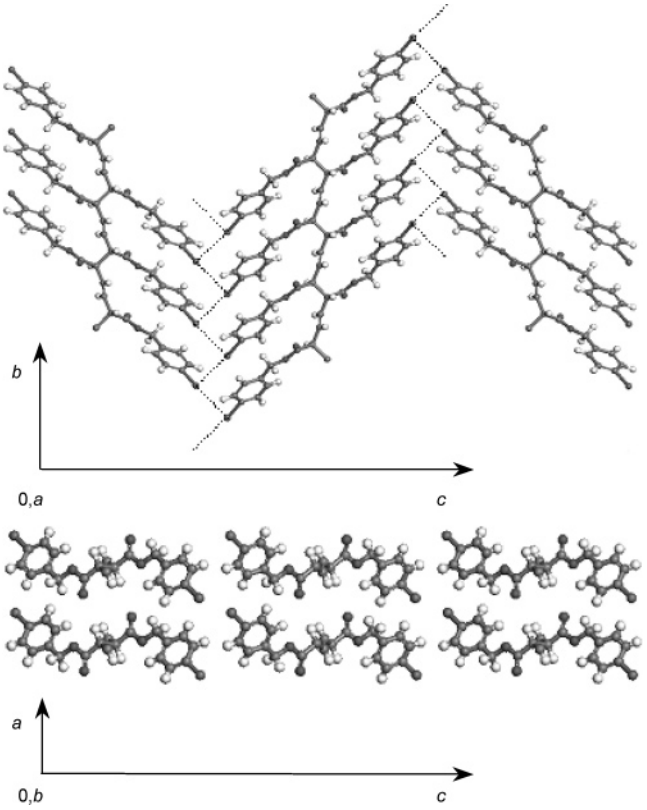

Figure 7. Crystal structure of poly(**1**) determined by single-crystal structure analysis at 30 °C: the view along the crystallographic *a* and *b* axes in the top and bottom, respectively. Dotted lines represent intermolecular halogen−halogen interaction.

Table 4. Crystallographic Data of Poly(1) and Poly(2)

compound	poly(**1**)	poly(**2**)
formula	$(C_{20}H_{16}O_4Br_2)_n$	$(C_{20}H_{16}O_4Cl_2)_n$
formula weight	480.15	391.25
crystal system	monoclinic	monoclinic
space group	$P2_1/c$	$P2_1/c$
a, Å	5.837(2)	5.6796(3)
b, Å	4.856(1)	4.8631(1)
c, Å	32.742(9)	32.097(1)
β, deg	91.05(2)	90.185(2)
V, Å^3	927.8(5)	886.54(5)
Z	2	2
ρ_{calc}, g/cm^3	1.719	1.466
total reflections	6690	5572
unique reflections	2095	2098
number observed	1456 ($I > 2\sigma(I)$)	1838 ($I > 2\sigma(I)$)
parameter ratio	11.56	12.94
R	0.064	0.066
R_w	0.091	0.170
GOF	1.20	1.70
$2\theta_{max}$, deg	54.9	54.9
temp, °C	30	23
ref	this work	23

and 1180 cm^{-1} are produced by $\nu(C^3-C^5) + \nu(C^5-O^7) + \nu(O^7-C^8)$ and $\nu(C^2-C^3) + \nu(O^7-C^8) + \nu(C^8-C^9)$, respectively (Figure 11).

The IR spectrum changed continuously from a temperature lower than the phase-transition temperatures observed by DSC or XRD experiments. Especially, the absorption bands related to the ester groups of the polymer side chain greatly changed as shown in Figure 10, in contrast to no significant change in peak position and shape in the bands due to the other bonds. These results suggest that the transition of the polymer crystal structure is first induced by conformational change in the local molecular structure of the polymer side chain at an initial stage, followed by a change accompanied by heat flow and then a drastic change in the crystal structures. It has already been revealed that the carbonyl groups interact with weak acidic hydrogens to cause C−H···O intermolecular interaction (weak hydrogen bond) in the polymer crystals of **1** or the other related benzyl ester compounds.[23,28,32] In this case, carbonyl interaction in a direction along the crystallographic *a*-axis becomes weaker upon heating, and rotation or any other change in the conformation around the ester groups would be induced. This local structural change may further induce a change in the crystal structure. A delay or difference in the structural changes observed between vibrational spectroscopy and diffraction data has been reported for the crystallization of flexible chain polymers, the phase transition of crystalline polymers, and polymerization processes.[3,33−36] The monitoring of a physical process by different measuring methods is very important to clarify the mechanisms of the phase transitions of polymer crystals.

In conclusion, we have demonstrated a novel phase transition of organic polymer crystals, which were directly fabricated by the topochemical polymerization of the corresponding diene monomers in the crystalline state. The highly regular crystalline structure of the polymer crystals has provided a new insight into organic crystalline materials on behalf of the thermal stability

Table 5. Comparison of Axis Lengths of Poly(1) Crystals for Three Phases[a]

temp (°C)	*a*-axis length (Å)	*b*-axis length (Å)	*c*-axis length (Å)
30	5.83 (5.83)	4.89 (4.88)	32.61 (32.69)
180	6.45 (6.44)	4.73 (4.72)	36.24 (36.19)
250	6.69	4.72	37.60
30	5.837[b]	4.856[b]	32.742[b]

[a] Axis lengths were evaluated from d_{002}, d_{102}, and $d_{11\bar{1}}$ spacings by XRD. Values in parentheses indicate an axis length observed during a cooling process from 250 to 30 °C. [b] Determined by single-crystal structure analysis.

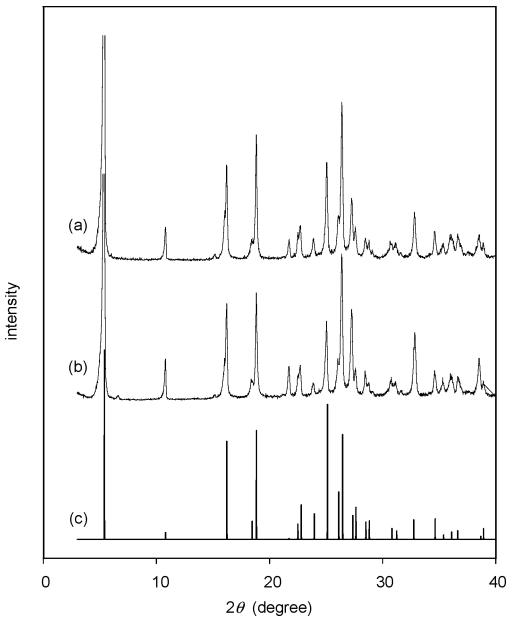

Figure 8. Comparison of observed and calculated XRD profiles: (a) before a heating and cooling process; (b) after a heating and cooling process; (c) calculated from the single-crystal structure.

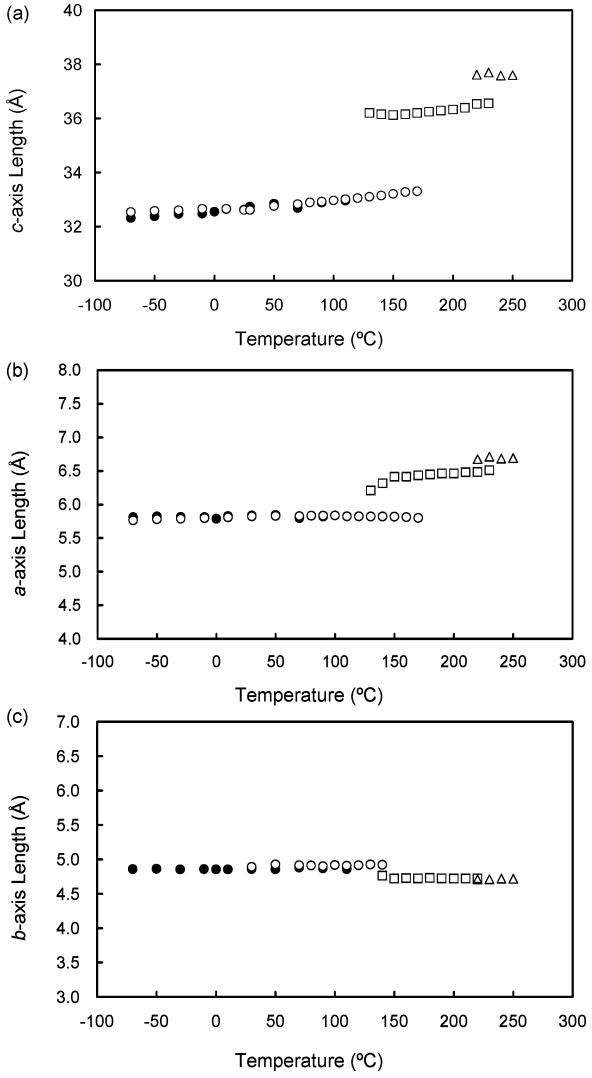

Figure 9. Change in axis lengths of poly(**1**) crystal during a heating process. Axis lengths were determined from d_{002}, d_{102}, and $d_{11\bar{1}}$ spacings in the XRD: (a) *c*-axis; (b) *a*-axis; (c) *b*-axis. Closed circles below 110 °C indicate the data determined by single-crystal structure analysis.

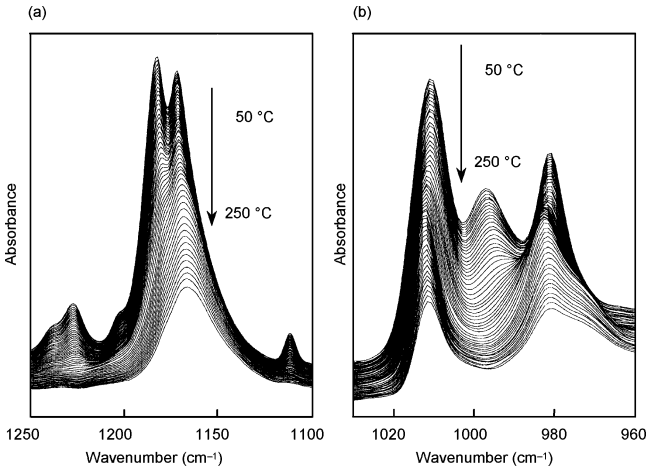

Figure 10. Change in expanded IR spectrum of poly(**1**): (a) 1100−1250 cm^{-1}; (b) 960−1050 cm^{-1} during a heating process from 50 to 250 °C at a heating rate of 10 °C/min.

of the polymer crystals, which are much superior to that of organic crystals consisting of low-molecular-weight molecules. It is not clear now whether similar reversible and multistep phase transition is observed for polymer crystals other than the muconate polymer crystals. However, topochemical polymerization implies the great potential to provide useful organic materials with sophisticated and completely regular structures of the polymer chains and crystals.

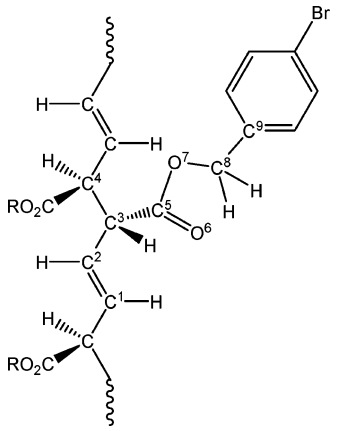

Figure 11. Numbering of constituent atoms of poly(**1**).

Acknowledgment. We gratefully thank Prof. Kohji Tashiro, Osaka University, for invaluable discussion, Rigaku Corp. for powder X-ray diffraction/DSC simultaneous measurements, JASCO Corp. for FT-IR measurements, and Prof. Kunio Oka, Osaka Prefecture University, for his kind assistance with the γ-radiation experiment. This work was supported by PRESTO-JST (Conversion and Control, 2000-2003) and the Grant-in-Aid Scientific Research on Priority Areas (Molecular Nano Dynamics, No. 16072215) from the MEXT, Japan.

Supporting Information Available: Single-crystal X-ray diffraction of poly(**1**) (CIF). The material is available free of charge via the Internet at http://pubs.acs.org.

References and Notes

(1) West, A. R. *Solid State Chemistry and Its Applications*: John Wiley & Sons: Chichester, 1984; p 417.
(2) Cheng, S. Z. D.; Keller, A. *Annu. Rev. Mater. Sci*. **1998**, *28*, 533−562.
(3) Tashiro, K.; Sasaki, S. *Prog. Polym. Sci.* **2003**, *28*, 451−519.
(4) Braga, D.; Grepioni, F. *Chem. Soc. Rev.* **2000**, *29*, 229−238.
(5) Moulton, B.; Zaworotko, M. J. *Chem. Rev.* **2001**, *101*, 1629−1658.
(6) Dunitz, J. D.; Bernsein, J. *Acc. Chem. Res.* **1995**, *28*, 193−200.
(7) Blagden, N.; Davey, R. J. *Cryst. Growth Des.* **2003**, *3*, 873−885.
(8) Samulski, E. T. *Physical Properties of Polymers*, 3rd ed.; Cambridge University Press: Cambridge, U.K., 2003; pp 316−380.
(9) Kato, T. *Science* **2002**, *295*, 2414−2418.
(10) Mandelkern, L. *Crystallization of Polymers*; Cambridge University Press: Cambridge, U.K., 2002; Vol. 1.
(11) Mandelkern, L. *Physical Properties of Polymers*, 3rd ed.; Cambridge University Press: Cambridge, U.K., 2003; pp 209−315.
(12) Desiraju, G. R. *Crystal Engineering: The Design of Organic Solids*; Elsevier: Amsterdam, 1989.
(13) Braga, D. *Chem. Commun.* **2003**, 2751−2754.
(14) Matsumoto, A.; Odani, T. *Macromol. Rapid Commun.* **2001**, *15*, 1195−1215.
(15) Matsumoto, A. *Polym. J.* **2003**, *35*, 93−121 and references therein.
(16) Tieke, B. *Adv. Polym. Sci.* **1985**, *71*, 79−151.
(17) Cheng, K.; Foxman, B. M.; Gersten, S. W. *Mol. Cryst. Liq. Cryst.* **1979**, *52*, 77−82.
(18) Xiao, J.; Yang, M.; Lauher, J. W.; Fowler, F. W. *Angew. Chem., Int. Ed.* **2000**, *39*, 2132−3235.
(19) Matsumoto, A.; Nagahama, S.; Odani, T. *J. Am. Chem. Soc.* **2000**, *122*, 9109−9119.

(20) Matsumoto, A.; Sada, K.; Tashiro, K.; Miyata, M.; Tsubouchi, T.; Tanaka, T.; Odani, T.; Nagahama, S.; Tanaka, T.; Inoue, K.; Saragai, S.; Nakamoto, S. *Angew. Chem., Int. Ed*. **2002**, *41*, 2502−2505.
(21) Itoh, T.; Nomura, S.; Uno, T.; Kubo, M.; Sada, K.; Miyata, M. *Angew. Chem., Int. Ed.* **2002**, *41*, 4306−4309.
(22) Hoang, T.; Lauher, J. W.; Fowler, F. W. *J. Am. Chem. Soc.* **2002**, *124*, 10656−10657.
(23) Matsumoto, A.; Tanaka, T.; Tsubouchi, T.; Tashiro, K.; Saragai, S.; Nakamoto, S. *J. Am. Chem. Soc.* **2002**, *124*, 8891−8902.
(24) Tashiro, K.; Nishimura, H.; Kobayashi, M. *Macromolecules* **1996**, *29*, 8188−8196.
(25) Nakamoto, S.; Tashiro, K.; Matsumoto, A. *Macromolecules* **2003**, *36*, 109−117.
(26) Tashiro, K.; Kariyo, A.; Nishimura, T.; Fujii, S.; Saragai, S.; Nakamoto, S.; Kawaguchi, A.; Matsumoto, A.; Rangsiman, O. *J. Polym. Sci., Part B, Polym. Phys.* **2002**, *40*, 495−506.
(27) Tashiro, K.; Nakamoto, S.; Fujii, T.; Matsumoto, A. *Polymer* **2003**, *44*, 6043−6049.
(28) Tanaka, T.; Matsumoto, A. *J. Am. Chem. Soc*. **2002**, *124*, 9676−9677.
(29) Matsumoto, A.; Tanaka, T. *Mol. Cryst. Liq. Cryst.*, in press.
(30) Stevens, E. D. *Mol. Phys*. **1979**, *37*, 27−45.
(31) Vonnegut, B.; Warren, B. E. *J. Am. Chem. Soc.* **1936**, *58*, 2459−2461.
(32) Desiraju, G. R.; Steiner, T. *The Weak Hydrogen Bond in Structural Chemistry and Biology*; Oxford University Press: Oxford, U.K., 1999.
(33) Hsu, S. L. In *Encyclopedia of Polymer Science*, 3rd ed.; Kroschwitz, Ed.; 2003; Vol. 8, pp 311−381.
(34) Tashiro, K.; Ueno, K.; Yoshioka, A.; Kobayashi, M. *Macromolecules* **2001**, *34*, 310−315.
(35) Bras, W.; Derbyshire, G. E.; Bogg, D.; Cooke, J.; Elwell, M. J. E.; Naylor, S. N.; Komanschek, B. E.; Ryan, A. J. *Science* **1995**, *267*, 996−999.
(36) Storov, A. A.; Penelle, J.; Hsu, S. L. *Macromolecules* **2000**, *33*, 6970−6976.

MA048905A